

FRET-FLIM at nanometer spectral resolution from living cells

Deepak K. Nair^{‡,†,*}, Mini Jose^{‡,†}, Thomas Kuner[§], Werner Zuschratter[‡], and Roland Hartig^{||}

[‡]Leibniz Institute for Neurobiology, Magdeburg, Germany

[§]Max Planck Institute for Medical Research, Heidelberg, Germany

^{||}Medical Faculty, Otto-von-Guericke University, Magdeburg, Germany

[†]Deepak K. Nair and Mini Jose contributed equally to this work.

*Correspondence: Deepak K. Nair, Leibniz Institute for Neurobiology, Brennekestrasse 6, 39118, Magdeburg, Germany, Tel: 0049-391-6263704, Fax: 0049-391-6263328,

kdeepak@ifn-magdeburg.de

Abstract: We report the investigation of Foerster's Resonance Energy Transfer dynamics in GFP based tandem constructs in living T-cells using a combination of Fluorescence Lifetime Imaging Microscopy (FLIM) and Fluorescence Lifetime Micro-Spectroscopy (FLMS) at picosecond time resolution and nanometer spectral resolution. The involvement of multiple lifetimes of CFP in energy transfer was analyzed by plotting pre-exponential factors of individual lifetimes along the wavelength resulting in the Decay Associated Spectra (DAS). A change in the amplitude of pre-exponential factors from positive to negative at the acceptor emission maxima was used as a confirmation of FRET in the multiexponential lifetime analysis.

©2006 Optical Society of America

OCIS codes: Time-resolved imaging (170.6920); Nanosecond phenomena (320.4240); Fluorescence Microscopy (180.1790); FRET-FLIM (999.9999)

References and links

1. Y. Chen, J. D. Mills, and A. Periasamy, "Protein localization in living cells and tissues using FRET and FLIM," *Differentiation* **71**, 528-541 (2003).
2. M. Elangovan, R. N. Day, and A. Periasamy, "Nanosecond fluorescence resonance energy transfer-fluorescence lifetime imaging microscopy to localize the protein interactions in a single living cell," *J. Microsc.* **205**, 3-14 (2002).
3. S. I. Murata, J. Kusba, G. Piszczek, I. Gryczynski, and J. R. Lakowicz, "Donor fluorescence decay analysis for energy transfer in double-helical DNA with various acceptor concentrations," *Biopolymers* **57**, 306-315 (2000).
4. M. Tramier, I. Gautier, T. Piolot, S. Ravalet, K. Kemnitz, J. Coppey, C. Durieux, V. Mignotte, and M. Coppey-Moisan, "Picosecond-hetero-FRET microscopy to probe protein-protein interactions in live cells," *Biophys. J.* **83**, 3570-3577 (2002).
5. J. W. Borst, M. A. Hink, A. V. Hoek, and A. J. W. G. Visser, "Effects of Refractive index and viscosity on Fluorescence and Anisotropy Decays of Enhanced Cyan and Yellow Fluorescent Proteins," *J. Fluoresc.* **15**, 153-160 (2005).
6. T. Kuner and G. J. Augustine, "A genetically encoded ratiometric indicator for chloride: capturing chloride transients in cultured hippocampal neurons," *Neuron* **27**, 447-459 (2000).
7. M. Ormo, A. B. Cubitt, K. Kallio, L. A. Gross, R. Y. Tsien, and S. J. Remington, "Crystal structure of the *Aequorea victoria* green fluorescent protein," *Science* **273**, 1392-1395 (1996).
8. J. R. Lakowicz, *Principles of Fluorescence Spectroscopy*, Second ed. (Kluwer Academic/Plenum Publishers, 1999).
9. J. R. Knutson, D. G. Walbridge, and L. Brand, "Decay-associated fluorescence spectra and the heterogeneous emission of alcohol dehydrogenase," *Biochemistry* **21**, 4671-4679 (1982).
10. L. Davenport, J. R. Knutson, and L. Brand, "Excited-state proton transfer of equilenin and dihydroequilenin: interaction with bilayer vesicles," *Biochemistry* **25**, 1186-1195 (1986).
11. I. Gautier, M. Tramier, C. Durieux, J. Coppey, R. B. Pansu, J. C. Nicolas, K. Kemnitz, and M. Coppey-Moisan, "Homo-FRET microscopy in living cells to measure monomer-dimer transition of GFP-tagged proteins," *Biophys. J.* **80**, 3000-3008 (2001).

12. K. Kemnitz, L. Pfeifer, R. Paul, and M. Coppey-Moisan, "Novel detectors for fluorescence lifetime imaging on the picosecond time scale," *J. Fluoresc.* **7**, 93–98. (1997).
 13. K. Kemnitz, L. Pfeifer, R. Paul, A. Fink, and A. Bergmann, "Time- and space correlated single photon counting Spectroscopy," in *Optical and Imaging Techniques for Biomonitoring*, H.-J. Foth, R. Marchesini, H. Podbielska M.D., M. Robert-Nicoud, H. Schneckenburger, eds., SPIE Proc. **2628**, 2-11 (1995).
 14. J. Lippincott-Schwartz and G. H. Patterson, "Development and use of fluorescent protein markers in living cells," *Science* **300**, 87-90 (2003).
 15. P. Kapusta, R. Erdmann, U. Ortmann, and M. Wahl, "Time-resolved fluorescence anisotropy measurements made simple," *J. Fluoresc.* **13**, 179-183 (2003).
 16. M. Tramier, K. Kemnitz, C. Durieux, and M. Coppey-Moisan, "Picosecond time-resolved microspectrofluorometry in live cells exemplified by complex fluorescence dynamics of popular probes ethidium and cyan fluorescent protein," *J. Microsc.* **213**, 110-118 (2004).
 17. R. R. Duncan, A. Bergmann, M. A. Cousin, D. K. Apps, and M. J. Shipston, "Multi-dimensional time-correlated single photon counting (TCSPC) fluorescence lifetime imaging microscopy (FLIM) to detect FRET in cells," *J. Microsc.* **215**, 1-12 (2004).
 18. W. Holzer, A. Penzkofer, M. Fuhrmann, and P. Hegemann, "Spectroscopic characterization of flavin mononucleotide bound to the LOV1 domain of Phot1 from *Chlamydomonas reinhardtii*," *Photochem. Photobiol.* **75**, 479-487 (2002).
 19. M. H. Seifert, D. Ksiazek, M. K. Azim, P. Smialowski, N. Budisa, and T. A. Holak, "Slow exchange in the chromophore of a green fluorescent protein variant," *J. Am. Chem. Soc.* **124**, 7932-7942 (2002).
 20. S. Habuchi, M. Cotlet, J. Hofkens, G. Dirix, J. Michiels, J. Vanderleyden, V. Subramaniam, and F. C. D. Schryver, "Resonance Energy Transfer in a Calcium Concentration-Dependent Cameleon Protein," *Biophys. J.* **83**, 3499–3506 (2002).
-

1. Introduction

Imaging interactions of proteins using Fluorescence Lifetime Imaging Microscopy (FLIM) is rapidly becoming an important tool to understand the biological functions of different macromolecules [1, 2]. FLIM is among the most efficient methods to measure Foersters Resonance Energy Transfer (FRET). In conventional FRET-FLIM studies the changes in donor decay have been studied extensively [3]. However by observing changes in donor decay alone, it is difficult to understand FRET occurring from the different conformational states of fluorophores like CFP which has been described to show multiexponential decays [4, 5]. Different emitting species of a fluorophore can possibly be involved in FRET causing different transfer times of the fluorophores measured as different lifetimes. Most of the investigations interpret lifetime decays based on mean lifetimes. Mean lifetimes however do not take into consideration the multiexponential components of the intensity decays, averaging them in the analysis.

Even though CFP and YFP are a most commonly used FRET pair the mechanism of energy transfer from different conformers of CFP remains unclear. In order to address this, genetically encoded tandem constructs [6] utilizing a variant of Yellow Fluorescent Protein, Topaz [7], as an acceptor together with Cyan Fluorescent Protein (CFP) as a donor were used. Simultaneous acquisition and analysis of donor and acceptor decays identified the lifetimes involved in energy transfer by modeling them with multiexponential decays. The acceptor decay kinetics only due to Resonance Energy Transfer will display the unique properties of an excited state reaction. In the time domain, the characteristics of an excited state reaction are a rise time in the decay characterized by negative amplitudes in the pre-exponential factors in the multiexponential analysis [8]. Modeling the decay kinetics of donor and acceptor simultaneously as a coupled excited state reaction allowed us to study the changes of pre-exponential factors and the fractional contributions of the individual decay components along the spectra. The plot of pre-exponential factors of different lifetimes arising from the fluorophores along the wavelength resulted in the Decay Associated Spectra (DAS) [9, 10].

A combination of the novel Delay Line (DL) and Quadrant Anode (QA) detectors based on Time and Space Correlated Single Photon Counting (TSCSPC) [4, 11, 12] in a single microscopy system was used for wide field non-scanning FLIM and Fluorescence Lifetime Micro-Spectroscopy (FLMS) in living cells. Simultaneous detection and global analysis of donor and acceptor fluorescence decays differentiated energy transfer dynamics between the

tandem constructs which differed in spacer lengths down to 8 amino acids. Here, in time domain FLIM, we present the importance of obtaining DAS at nanometer spectral resolution in living cells to understand the complex multiexponential decays of donor and acceptor molecules involved in excited state reactions like energy transfer.

2. Materials and methods

2.1 Cloning and transfections

CFP and Topaz were fused with a linker consisting of 24 amino acids residues (Clomeleon [6]) (KLTGSGSGENLYFQGGGSGGTSST). Instead of the 24 amino acid linker, constructs with shorter linkers contained 8 (KLTGTSST) or 16 (KLTGENLYFQGGTSST) amino acid residues. All constructs were verified by sequence analysis. The constructs with 24 amino acid spacer will be referred as C24T and the variants with 8 amino acids and 16 amino acids will be referred as C8T and C16T. Jurkat T-cells were transfected with 20 μg of cDNA of the different FRET constructs: C24T, C16T, C8T and pECFP (Clontech, Mountain View, CA) using an electroporation system gene pulser[®] II (BioRad, Hercules, CA).

2.2 TSCSPC

The TSCSPC method and the technical aspects regarding the detectors (Europhoton GmbH, Berlin, Germany) have been described elsewhere [12, 13]. However we present the implementation of the detectors Delay line (from now on referred to as point detector) and Quadrant Anode (from now on referred to as imaging detector) in FLIM and FLMS setup.

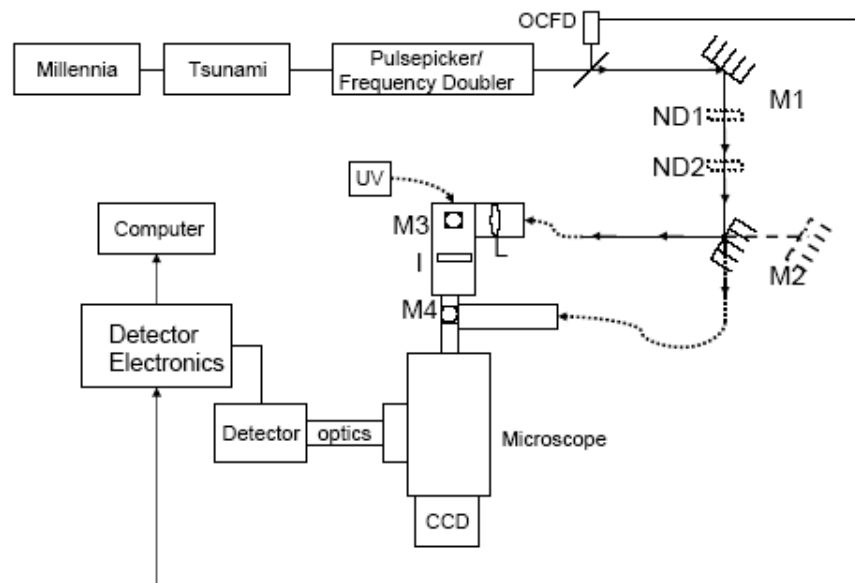


Fig. 1. Picosecond FLIM setup for simultaneous detection of donor and acceptor lifetimes using both point and imaging detectors. OCFD: Optical Constant Fraction Discriminator triggered by laser pulse, M: mirrors, ND: neutral density filters, UV: UV lamp for steady state imaging, L: planar convex lens, I: iris to control the area of excitation of the sample and CCD: Charge Coupled Device.

2.3 FLIM-FLMS

The experimental setup is shown in Fig. 1. A femtosecond Titanium sapphire laser (Tsunami, Model 3955, 690-1080 nm, 80 MHz, Spectra Physics, Mountain View, CA), pumped by a continuous wave visible diode laser (Millennia Vs, 5W, TEM₀₀ 532 nm, Spectra Physics) was

tuned and frequency doubled using a frequency doubler/pulse selector (Model 3986, Spectra Physics) to a wavelength of 420 nm with a pulse repetition rate of 8 MHz. This wavelength was optimal to excite the donor CFP to at least 80% and the acceptor YFP to less than 5% [14]. Since the fluorescence decays of the fluorophores used (CFP, Topaz) are in the range of 1-5 ns the repetition rate of the excitation pulses (125 ns) provided the fluorophores enough time to relax back to the ground state before they are excited by the next pulse. About 10% of the laser output from the frequency doubler/pulse selector was used to trigger the Optical Constant Fraction Discriminator (OCFD 401, Becker and Hickl, Berlin, Germany) to determine the stop pulse of the excitation beam to the electronics of the detectors. The laser beam was guided by mirror M1 to two circular variable neutral density filters ND1 and ND2 (Thorlabs, Karlsfeld, Germany) which were arranged in series to control the power of the laser beam. The laser beam was coupled alternatively via two optical fibres mounted on a three dimensional micrometer stage (Thorlabs) to different ports of an inverted microscope (IX81, Olympus, Hamburg, Germany) to illuminate the sample either for the point detector or the imaging detector. Switching between the different excitation paths was performed using the manually switchable mirror M2.

The point detector needs a point or a very small excitation area so that it can selectively collect photons from a small defined region within a cell. The collimated laser beam from the fibre output was focused by a convex lens, L, ($f=+150$ mm) (Edmund Optics, Karlsruhe, Germany) decreasing the area of illumination for the excitation beam. The region of interest was selected by closing an iris (I) within the excitation path around the beam to limit the area of excitation. The laser beam was finally focussed onto the sample using an oil immersion 100x objective (Plan Apo 100x/1.45 oil, TIRFM, Olympus) after passing a beam splitter 450 DCLP (AHF Analysentechnik, Tuebingen, Germany). The fluorescence emission from the tiny selected area passed an emission filter HQ 460 ALP (AHF Analysentechnik) and a slit (11 mm x 0.10 mm) of a polychromator fixed in front of the sensitive area of the point detector to translate the spectrally resolved intensity decays on the detector.

In the alternate path, the collimated beam from the optical fibre was used to provide whole field illumination for the imaging detector. A manually switchable mirror M4 was used to alternate between the illumination ports for the point and imaging detectors. The collimated beam passed the beamsplitter 450 DCLP (AHF Analysentechnik) and illuminated the back focal plane of the 100x objective. The fluorescence was collected via the objective and was reflected to the side port of the microscope after passing an emission filter HQ 460 LP. The detectors were used alternatively in combination with the optics suited for each detector. The point detector was used in combination with a polychromator. In front of the imaging detector, a Dual Image (Europhoton GmbH, fluorescence filters and beamsplitter from AHF Analysentechnik) was mounted to split the fluorescence into two specific cut off wavelength bands via a beamsplitter (dichroic 505 DCXR). Two bandpass filters defined the width of the wavelength bands of the donor (CFP: D 480/40 M) and the acceptor (YFP: 540/40 ALP). These two fluorescence bands illuminated two different areas of the imaging detector collecting the dynamics of donor and acceptor simultaneously. QA capture software (Europhoton GmbH) was used to control the data acquisition of the imaging detector. Measurements were performed continuously by acquiring the photons for a certain time to achieve a good signal to noise ratio. The imaging detector was cooled throughout the measurements to avoid over heating. The excitation power used to illuminate samples was less than $100 \mu\text{W}/\text{cm}^2$ (measured by a laser power meter, PD-300-3W, Ophir Optronics GmbH, Rohrsen, Germany), minimizing photobleaching effects for long term observation.

2.4 Steady state imaging

Images of the cells were acquired using a CCD camera (F-View, SIS Imaging Systems GmbH, Duesseldorf, Germany) connected to the top port of the microscope (Fig. 1). The CFP and Topaz signals were collected by filter settings (excitation, dichroic, and emission, AHF

Analysentechnik), D 436/20, 455 DCLP, and D 480/40 for CFP and HQ 500/20, Q 515 LP, and HQ 535/30 for Topaz. Only cells showing moderate fluorescence intensity of the transfected constructs were used for imaging and FLIM-FLMS.

2.5 Data analysis

Calibration of the setup was performed to determine time channel resolution of the point (24.8 ps/channel) and imaging detector (9.7 ps/channel) with known delays. Wavelength calibration of the point detector (1.02 nm/channel) was calculated from known emission lines of a Xenon lamp (6035 Hg (Ar), Oriel Instruments, Stratford, CT). To obtain lifetimes from fluorescence decays, the experimental measurements were modeled by the convolution product of a multi-exponential theoretical model with the instrument response function (IRF): $i(t) = \text{IRF}(t) \otimes \sum \alpha_i e^{-t/\tau_i}$, where α_i is the relative contribution of fluorescent species, characterized by the fluorescence lifetime τ_i and IRF is the measurement of the pulsed excitation obtained by acquiring the reflection of the laser beam to the detector. Data were analyzed by Levenberg-Marquardt non-linear least-squares algorithm using the Globals Unlimited software package (version 1.20) developed at the Laboratory for Fluorescence Dynamics at the University of Illinois at Urbana-Champaign.

Data acquired by the point detector were fit with linked lifetimes along different decays corresponding to different emission wavelengths. The decays were obtained by gathering data over a fixed number of continuous wavelength channels via addition of blocks of wavelength channels equivalent to 6.12 nm. The contribution of the lifetimes in the intensity decays were calculated from pre-exponential factors. The pre-exponential factors of lifetimes were plotted at different wavelengths resulting in the Decay Associated Spectrum (DAS). The comparison of DAS of different multiexponential components allowed us to discriminate the fluorescent species involved in different excited state processes. Data collected by the imaging detector were analyzed by selecting corresponding regions of interests for the CFP and Topaz channels as defined by the filter settings of the Dual Image.

The data sets acquired by the detectors were exported to the Globals Unlimited software format. The donor and acceptor decays were analyzed with linked lifetimes. The quality criterion of the global fit was defined as $\chi^2 < 1.3$ for all analyzed decays. The criterion for improvement of χ^2 on addition of multiexponential components was set to a value of $\Delta\chi^2$, the ratio between the χ^2 of the previous model and the current model after the addition of a single lifetime component, where $\Delta\chi^2 > 1.05$. The values of χ^2 were checked by using the linked multiexponential model and the unlinked model and the data were discarded if the ratio of χ^2 s was greater than 1.05, indicating a random error originating from the data acquisition. The intensity decays of independent control measurements of coumarin6 at magic angle were observed to be monoexponential with lifetimes of 2.30 ns for the point detector and 2.29 ns for the imaging detector, which were in agreement with the published value of 2.30 ns [15].

In the time domain, the energy transfer efficiency is calculated by $E = 1 - \tau_{DA} / \tau_D$ where τ_{DA} is the mean lifetime of the donor in the presence of an acceptor and τ_D is the unperturbed mean lifetime of the donor. The mean lifetime τ_{mean} of a multiexponential fluorophore is calculated as $\tau_{\text{mean}} = \sum \alpha_i \tau_i / \sum \alpha_i$, where τ_i is the lifetime and α_i is the corresponding pre-exponential factor. α_i and τ_i are determined by global analysis. The pre-exponential factor α_i of intensity decay is positive except in the case of excited state reactions where the pre-exponential factors changes to a negative sign [8]. α_i was plotted along the wavelength to obtain the DAS. The fractional contributions of different lifetimes in the intensity decay were calculated from the pre-exponential factors of the multiexponential model as $\alpha_i / \sum \alpha_i$.

Rigorous error analysis using the global analysis program was performed to obtain a realistic estimation of the variation of χ^2 associated with each lifetime. A set of intervals was defined for each lifetime in the model performing a complete set of analysis. The examined parameter was fixed at the current trial value, but all other parameters were allowed to vary to minimize the value of χ^2 . A plot of the change of χ^2 with the change in lifetimes was obtained.

Comparison of these results with the obtained multiexponential model was used to judge the quality of lifetimes in the fit.

3. Results

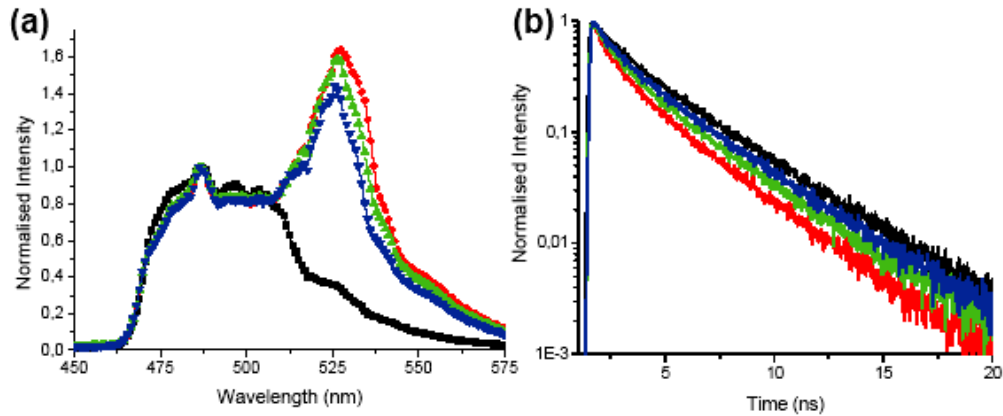


Fig. 2. (a). Comparison of representative fluorescence emission spectra of ECFP (black) and the size variants of tandem constructs C8T (red), C16T (green) and C24T (blue). (b) Comparison of fluorescence intensity decays of ECFP and the size variants of tandem constructs at the emission maximum of CFP in a band of 483.8 ± 3.06 nm. Control ECFP (black), C8T (red), C16T (green) and C24T (blue). The intensity decays of FRET variants were faster compared to ECFP. The fastest decay was detected in the case of C8T indicating best FRET efficiency. The intensity decays had 10^4 counts at the maximum with $\chi^2 < 1.3$.

3.1 Fluorescence dynamics of ECFP in T-Lymphocytes

In order to understand the fluorescence dynamics of ECFP as a donor, living T-Lymphocytes expressing ECFP ($n=6$) were measured. The ECFP fluorescence emission spectrum yielded an emission maximum at 486 ± 1.02 nm [Fig. 2(a)] and the lifetime analysis was performed between 468 nm and 590 nm. For this purpose, the spectrum was divided into 20 bands of 6.12 nm each and the deconvolution of intensity decays of ECFP yielded two lifetimes of 3.37 ± 0.03 ns and 1.06 ± 0.03 ns. At the emission maximum of ECFP, the τ_1 and τ_2 showed contributions of $60 \pm 2\%$ and $40 \pm 2\%$ respectively [Fig. 2(b)] which resulted in a mean lifetime of 2.44 ± 0.08 ns. The pre-exponential factors obtained for individual lifetimes were plotted along the wavelength to yield the DAS of ECFP [Fig. 3(a)]. Comparison of the DAS for both the lifetime components showed a similar pattern indicating that these originated from the same fluorophore. Due to the absence of excited state reactions in ECFP alone the pre-exponential factors of all the lifetime components in the intensity decays remained positive. The plot of the percentage of contributions of the two ECFP lifetimes along the wavelength revealed a slight reduction in the contribution of the τ_1 [Fig. 3(b)] and a corresponding increase in the τ_2 with increasing wavelength. These results were consistent with previous reports [16, 17], indicating that CFP expressed in living cells can be modeled with two exponential decays. The resulting mean lifetimes of ECFP were also calculated for different wavelength channels and were plotted [Fig. 3(c)].

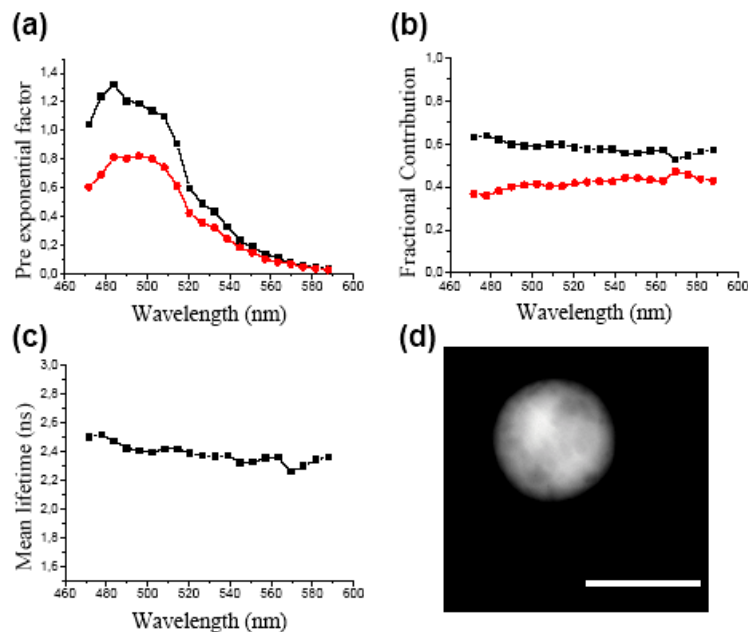


Fig. 3. (a). Decay Associated Spectrum of ECFP. Intensity decays of all measurements were analyzed in 20 emission bands from 470 nm to 590 nm and the pre-exponential factors of lifetimes 3.37 ± 0.03 ns (black) and 1.06 ± 0.03 ns (red) were plotted along the wavelength. (b) The contributions of both the lifetimes 3.37 ± 0.03 ns (black) and 1.06 ± 0.03 ns (red) were calculated and plotted as normalized fractional contribution from the pre-exponential factors along the wavelength. (c) Mean lifetimes of intensity decays of the emission bands were plotted along the wavelength (d) CCD image of Jurkat T-cell expressing ECFP (bar: 10 μ m).

3.2 Fluorescence emission spectra of tandem constructs

The different size variants of the tandem constructs, C8T, C16T and C24T, with the number of amino acids varying from 8 to 24 in the spacers separating the fluorophores, were used to study the photophysical mechanism behind resonance energy transfer from CFP to Topaz. Topaz is a variant of YFP which show similar absorption and emission spectra as YFP [6]. The emission spectra of the different constructs were plotted after normalizing them at the CFP peak [Fig. 2(a)]. The ratios of intensity (R) at the Topaz emission peak (527.3 ± 1.02 nm) to the CFP emission peak (486.4 ± 1.02 nm) were calculated for the different constructs. C8T showed highest R values of all the constructs of 1.69 ± 0.35 whereas C24T showed smallest R values of 1.49 ± 0.20 with C16T exhibiting R values of 1.56 ± 0.25 . These values were calculated from independent measurements of transfected cells (n=9).

3.3 Fluorescence lifetime dynamics of tandem constructs

All measurements were performed using the point detector unless otherwise stated. The lifetime analysis was done similar to the control ECFP and the pre-exponential factors of the lifetimes were plotted along the wavelength resulting in the DAS of the FRET constructs. The percentage of contributions of different lifetimes and the mean lifetimes were calculated for intensity decays of different wavelength bands along the spectrum (Table 1).

The fluorescence decays from living Jurkat T-cells (n=5) expressing the different tandem constructs were fit with a three exponential model. Modeling with four exponentials did not significantly improve the χ^2 or the fit. The multiexponential lifetimes obtained from the analysis were very similar between the constructs. Interestingly, the contribution of the

individual lifetimes at the donor emission maxima showed a dramatic change with changes in spacer lengths (Table 1). The contribution of τ_3 was observed to decrease with increasing spacer lengths in contrast to those of τ_1 and τ_2 , which showed a simultaneous increase for the same. This resulted in increased mean lifetimes for C24T, while C8T showed the lowest mean lifetime among the constructs. The difference was also clear from the plots of the overall donor fluorescence decays of the different constructs as shown in Fig. 2(b). The fluorescence decays of all the FRET constructs at the donor emission maxima (483.8 ± 3.06 nm) were shorter compared to control ECFP, with C8T showing the shortest among them.

Table 1: Multiexponential lifetimes and the percentage of contributions of each lifetime for ECFP and CFP of different size variants of tandem constructs

Construct	τ_1 [ns]	τ_1 [%]	τ_2 [ns]	τ_2 [%]	τ_3 [ns]	τ_3 [%]	τ_{mean} [ns]	n^a
ECFP	3.37 ± 0.03	60 ± 2	1.06 ± 0.03	40 ± 2			2.44 ± 0.08	6
C8T	3.39 ± 0.03	24 ± 5	1.31 ± 0.07	30 ± 1	0.16 ± 0.02	46 ± 4	1.27 ± 0.12	5
C16T	3.41 ± 0.04	27 ± 3	1.32 ± 0.04	33 ± 1	0.16 ± 0.02	41 ± 4	1.41 ± 0.12	5
C24T	3.42 ± 0.02	31 ± 3	1.35 ± 0.04	35 ± 2	0.19 ± 0.02	35 ± 3	1.59 ± 0.09	5

^a number of independent measurements are denoted as n

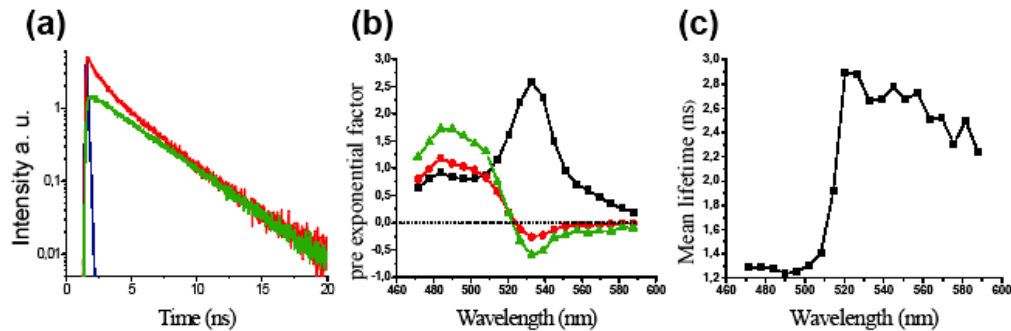


Fig. 4. (a). Comparison of CFP and Topaz decays in C8T. The intensity decay of donor CFP (red) in a band of 483.8 ± 3.06 nm and the intensity decay at Topaz (green) emission maximum in a band of 527.3 ± 3.06 nm. (b) DAS of C8T. The decays were fit with a three exponential model with lifetimes of 3.39 ± 0.03 ns (black), 1.31 ± 0.07 ns (red) and 0.16 ± 0.02 ns (green). Intensity decays of all measurements were analyzed in 20 emission bands from 470 nm to 590 nm. At the emission maximum of Topaz (between 520 and 540 nm) the pre-exponential factors of two lifetimes were negative indicating the presence of excited state reactions. (c) Mean lifetimes of intensity decays were calculated along the emission bands and were plotted along the wavelength. A sharp increase was observed for the mean lifetimes at the emission maximum of Topaz. The intensity decays had 10^4 counts at the maximum with global $\chi^2 < 1.3$.

The acceptor decays of the FRET constructs were completely different from their corresponding donor dynamics as observed in Fig. 4(a). The DAS showed negative pre-exponential factors for the two short components, τ_2 and τ_3 , near the emission maximum of Topaz [Figs. 4(b), 5(a), 5(b)]. An increase in the contribution of the long lifetime component,

τ_1 , and a subsequent reduction in the contribution of the two short lifetime components near the emission maximum of the acceptor were observed. For C8T, at the acceptor emission maximum, the contributions of the lifetimes, τ_1 , τ_2 and τ_3 (Table 1) were $86 \pm 4\%$, $8 \pm 5\%$ and $6 \pm 5\%$ respectively, which resulted in a sharp increase of mean lifetimes from 1.27 ± 0.12 ns to 3.03 ± 0.11 ns from the donor towards the acceptor emission maxima along the spectra [Fig. 4 (c)].

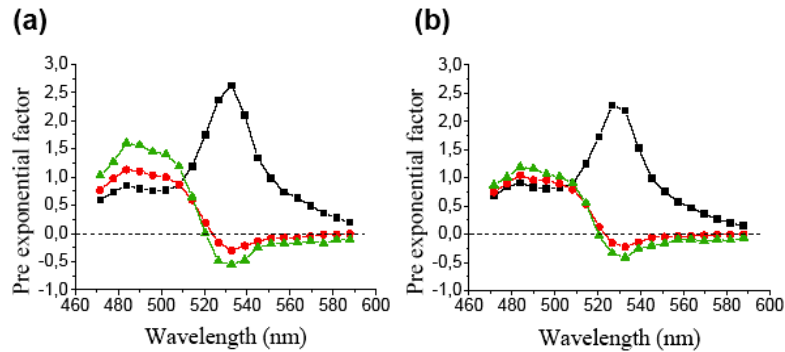


Fig. 5. Comparison of DAS for different tandem constructs showed a significant increase in the contributions of τ_1 and τ_2 and a corresponding reduction in the contribution of τ_3 with increase in spacer length. Intensity decays of all measurements were analyzed in 20 emission bands from 470 nm to 590 nm. (a) Plot of DAS for C16T with pre-exponential factors of the lifetimes 3.41 ± 0.04 ns (black), 1.32 ± 0.04 ns (red) and 0.16 ± 0.02 ns (green). (b) Plot of DAS for C24T with pre-exponential factors of the lifetimes 3.42 ± 0.04 ns (black), 1.35 ± 0.04 ns (red) and 0.19 ± 0.02 ns (green). The intensity decays had 10^4 counts at the maximum.

For C16T and C24T, changes in the contributions of the lifetimes were also observed for the acceptor channels compared to C8T. This resulted in acceptor mean lifetimes of 3.11 ± 0.09 ns and 3.14 ± 0.08 ns for C16T and C24T respectively. The plot of mean lifetimes showed an increase from the donor to the acceptor channels along the wavelength, similar to C8T.

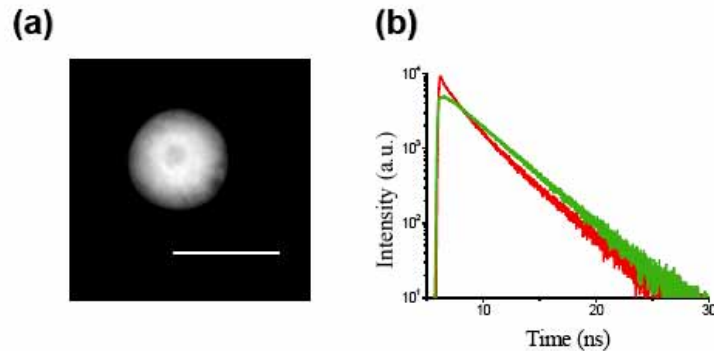


Fig. 6. Simultaneous analysis of donor and acceptor intensity decays in Jurkat T-cells expressing C8T collected by the imaging detector. The wide field fluorescence emission signal was split into two wavelength bands of CFP and Topaz with Dual Image to detect simultaneously the time resolved images of donor and acceptor. (a) CCD image of the Jurkat cell (bar: $10 \mu\text{m}$). (b) Simultaneous analysis of donor and acceptor probes namely, CFP (red) and Topaz (green): Analysis resulted in three lifetimes of 3.23 ns, 1.24 ns and 0.21 ns with the pre-exponential factors of the 0.21 ns showing negative amplitudes for the C8T. The local χ^2 values for the linked and unlinked analysis of the donor decay were 1.17 and 1.16. The lifetimes obtained for unlinked donor were 3.17 ns, 1.17 ns and 0.17 ns.

The lifetime dynamics of C8T in living T-cells ($n=4$) using the imaging detector [Fig. 6(b)] showed a three exponential model analogous to the results from the point detector and the lifetimes obtained were 3.25 ± 0.03 ns, 1.29 ± 0.06 ns and 0.22 ± 0.03 ns [Fig. 6(b)]. The percentage of contributions of these lifetimes was similar to the data obtained from the point detector. Within the donor band, the three lifetime components contributed to $23 \pm 3\%$, $34 \pm 1\%$ and $43 \pm 3\%$ respectively in contrast to the contributions of $83 \pm 3\%$, $6 \pm 3\%$ and $10 \pm 6\%$ in the acceptor band. Rigorous error analysis was done to investigate the realistic spread of χ^2 with changes in the lifetime. The lifetimes obtained from global analysis were comparable to the minimum of χ^2 as shown in Fig. 7. The mean lifetimes in the donor and acceptor bands were 1.28 ± 0.08 ns and 2.82 ± 0.15 ns.

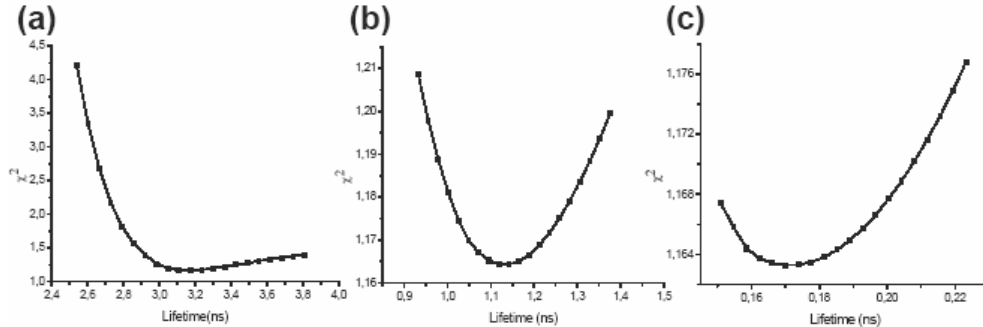


Fig. 7. Rigorous error analysis was performed for different lifetime components obtained for the intensity decay of the donor. The changes in χ^2 over the changes in lifetimes were plotted to check the quality of the lifetimes obtained from global analysis. The minimum of the curve was detected to be comparable to the values obtained from the multiexponential analysis. The donor decay of C8T from Fig 5 is presented as an example. (a) χ^2 variation of the 3.17 ns component for the unlinked donor decay. (b) χ^2 variation of the 1.17 ns lifetime in the unlinked donor decay. (c) χ^2 variation of the short lifetime component (0.17 ns) for the unlinked donor decay .

Using the imaging detector, negative pre-exponential factors were observed only for τ_3 in contrast to the negative amplitudes of τ_2 and τ_3 using the point detector. This could be attributed to the usage of filters with a bandwidth of 40 nm to detect the donor and the acceptor emission in the imaging detector while the point detector combined a long pass filter and the polychromator for a wavelength resolution of continuous bands of 6.12 nm. Therefore the effects would be averaged out in the imaging detector due to the broader wavelength detection bands. The imaging detector was used as an independent system to check the reliability of lifetimes obtained from the point detector at a better time resolution. Since the analysis resulted in similar lifetimes in imaging and point detector with the latter showing better wavelength resolution, the studies on the different size variants of tandem constructs were based on the measurements from the point detector alone.

Co-expressing individual ECFP and Topaz molecules resulted in DAS showing positive amplitudes for the pre-exponential factors of all the lifetimes, indicating the absence of energy transfer. The mean lifetimes obtained in this case were similar to that of control ECFP, indicating that fluorescence emission characteristics of CFP were not perturbed in the presence of acceptor molecules when they were not within the Foerster radius (data not shown). The direct excitation of cells expressing the acceptor molecules alone with 420 nm resulted in lifetimes of 2.93 ± 0.02 ns and 0.03 ± 0.01 ns. The DAS obtained from YFP analysis in cells showed the origin of the short lifetime to be different from that of the 2.93 ns component. Autofluorescence measurements in untransfected cells were modeled with 3 exponentials with lifetimes of 4.38 ± 0.60 ns, 0.74 ± 0.04 ns and 0.04 ± 0.01 ns with corresponding contributions of $6 \pm 1\%$, $12 \pm 2\%$ and $82 \pm 3\%$ respectively. The similarity of

these lifetimes with those obtained from YFP expressing cells allowed us to propose, the short component of the latter to be originating from autofluorescence molecules and the source of the long lifetime of 2.93 ns to be the deprotonated species of YFP. Flavin molecules can be considered as a major source of autofluorescence. With the excitation wavelength used, YFP was excited less than 5% [14] while the Flavin molecules were excited more than 70% [18]. Deeper investigations of the control acceptor decays was not possible due to the lack of direct excitation of the deprotonated band of Topaz in the current experimental setup.

4. Discussion

In living cells, the excited state energy transfer from CFP to Topaz, a spectral variant of YFP was studied at picosecond time resolution and nanometer spectral resolution in the time domain using a combination of Fluorescence Lifetime Imaging Microscopy (FLIM) and Fluorescence Lifetime Micro-Spectroscopy (FLMS). For this purpose, a microscope system was successfully developed based on TSCSPC technique combining wide field non-scanning point and imaging detectors to measure FLMS and FLIM respectively. This allowed an alternative study of the fluorescence lifetimes at high temporal resolution as a function of wavelength or space. Long-term observation of samples without photobleaching was possible due to the minimal invasive excitation intensities, less than 100 $\mu\text{W}/\text{cm}^2$.

Table 2 Efficiency of energy transfer occurring from CFP of different size variants of the tandem constructs^a

Construct	E τ_{mean} [%]	R
C8T	48 \pm 10	1.69 \pm 0.35
C16T	42 \pm 9	1.56 \pm 0.25
C24T	35 \pm 6	1.49 \pm 0.20

^a FRET efficiencies (E) were calculated from mean lifetimes of each construct which were in direct relationship with R values calculated from the ratio of Topaz to CFP peaks in the emission spectra of different tandem constructs.

DAS of all the different tandem constructs [Figs. 4(b), 5(a) and 5(b)] revealed negative amplitudes for the pre-exponential factors corresponding to the two short lifetime components at the emission maximum of the acceptor. The co-expression of donor and acceptor molecules or the expression of CFP or YFP alone showed only positive pre-exponential factors, indicating the absence of excited state reactions. Comparison of the DAS of the lifetimes for the different constructs revealed the maximum contribution of τ_3 for the shortest construct C8T, which decreased with increasing spacer lengths connecting the fluorophores, with a subsequent increase in the contribution of the longer lifetimes. This in turn resulted in lowest mean lifetimes for the C8T construct, though the mean lifetimes of all the FRET samples were considerably decreased compared to the control ECFP (Table 1). Calculation of FRET efficiencies from the mean lifetimes indicated a decrease with increase in spacer lengths from 48% (C8T) to 35% (C24T) as shown in Table 2. The analysis of the mean lifetimes along the spectra showed a drastic increase near the acceptor emission maximum, which was attributed to the occurrence of an excited state reaction resulting in the reduction of mean lifetimes of the donor and a subsequent increase in the mean lifetimes of the acceptor.

From the DAS of the tandem FRET constructs, it was perceived that two lifetimes were involved in energy transfer, which could arise from the two conformational states of the CFP molecules. The two conformers of CFP can act as two different donors [19], which can

independently be involved in energy transfer [5]. Since CFP is biexponential, it was expected to show at least four lifetimes in its intensity decay when involved in energy transfer. It was possible to fit the fluorescence decays of FRET constructs with a three exponential model. According to the proposed model of CFP, the participation of τ_1 of CFP in energy transfer results in a lifetime close to its τ_2 , whereas the involvement of τ_2 of CFP in FRET results in a still shorter lifetime. τ_1 of the FRET constructs were very close to the τ_1 of unperturbed CFP (Table 1). This indicated that a subpopulation of the donor probes cannot efficiently undergo energy transfer. Topaz is sensitive to high anionic concentrations. In living T-lymphocytes the physiological intracellular chloride concentration is low; between 10-20 mM (unpublished data). The binding of chloride ions to the anionic chromophore of Topaz can hinder it from receiving energy from the CFP molecules. This would result in a fraction of CFP molecules to show unperturbed lifetimes. Thus τ_1 in the FRET constructs would indicate those CFP molecules not involved in any excited state reaction. However resolving the τ_2 of CFP not involved in energy transfer was more difficult. τ_2 of the FRET constructs was longer than the τ_2 of unperturbed CFP (Table 1), indicating that this could consequently be a mix of the unperturbed τ_2 of CFP and a FRET lifetime occurring from the τ_1 of CFP, further verifying our foresaid model, agreeing with the three exponential modeling of the FRET constructs.

The negative amplitudes in the intensity decays of the acceptor is characteristic of excited state reactions when measured in the time domain, arising only due to the presence of energy transfer from CFP to Topaz. The direct excitation of YFP in its deprotonated band, in the absence of excited state reactions, yield monoexponential decays [20]. When involved in FRET, YFP accepts energy from CFP molecules by coupling of excited states resulting in an increase in the excited state species of YFP. This increase is an excited state growth process in contrast to the normal decay processes [9, 10]. The pre-exponential factors of the multiexponential lifetimes involved in this excited state growth process will be opposite in sign (negative) compared to that of the normal decay processes (positive). In this case, the excited state of YFP can be populated by two different conformers of CFP at the same or different rates, characteristic of the excited state dynamics of the individual conformers of CFP. At the acceptor emission maxima, two lifetimes can show negative pre-exponential factors indicating two different rate processes from these conformers of CFP, populating the excited state of YFP. Upon reaching an excited state equilibrium, the YFP molecules relax back to the ground state with its natural lifetime.

The multiexponential decays at the acceptor emission maxima were modeled with three lifetimes. The lifetimes τ_2 and τ_3 in the FRET constructs were different from the unperturbed donor lifetimes (Table 1). It was observed that these multiexponential lifetimes show negative pre-exponential factors at the acceptor emission maximum from 520 nm to 545 nm, indicating that the Topaz molecules can accept energy from multiple conformers of CFP. Thus the fluorescence decays of CFP and YFP were modeled with three exponentials. The multi-exponential modeling of the different FRET constructs along with DAS was sufficient to understand the photophysics of energy transfer occurring from CFP to Topaz in these tandem constructs.

Calculation of mean lifetimes of different constructs showed that τ_{mean} of the FRET constructs increased with increasing spacer lengths. However τ_{mean} does not discriminate the free donor fluorophores not involved in energy transfer. This information is averaged when calculating the mean lifetimes from the multiexponential analysis. Usually a reduction in mean lifetimes or an additional multiexponential component is regarded as an occurrence of energy transfer. These parameters could also be influenced by changes in pH and ionic concentrations in living cells (Jose et al., unpublished data). Therefore, a simultaneous analysis of donor and acceptor decays was essential to distinguish energy transfer from other cellular effects. Together with the changes in the sign of the pre-exponential factors along the wavelength as observed from the DAS, and changes of mean lifetimes from the donor to the acceptor region, the presence of FRET from multiple conformations of CFP to Topaz was

confirmed and the distinction of the FRET dynamics in the constructs which differed only in 8 amino acids was successful.

5. Conclusion

The FLIM-FLMS system was used to collect donor and acceptor dynamics at nanometer spectral resolution and picosecond temporal resolution to calculate DAS. Simultaneous detection and analysis of emission spectra and lifetimes of donor and acceptor molecules provided better information to discriminate excited state reactions like energy transfer, charge transfer and dimerization from cellular artefacts like autofluorescence. Most of the fluorophores used in FRET studies in living cells are multiexponential in nature. Therefore, it is essential to understand how the different conformations of single fluorophores like CFP can be involved in FRET. DAS is a powerful tool to study the FRET occurring from multiple conformations and can thus discriminate between different fluorescent species involved in FRET, which is not possible by using mean lifetimes. With our experimental set up, it was possible to distinguish FRET between GFP based tandem constructs, when the spacer lengths differed only in 8 amino acids. FRET techniques using FLIM-FLMS will be a useful tool to predict the conformations of different proteins in living cells and to study macromolecular interactions in their natural environment.

Acknowledgments

The authors are grateful to Dr. Karl-Heinz Smalla and Dr. Ulrich Thomas, Leibniz Institute for Neurobiology, Magdeburg for helpful discussions. We acknowledge Dr. Ronald Steffen, Australian National University, Canberra, Australia for helpful discussions on the model and data. The authors thank Kathrin Gruss, Leibniz Institute for Neurobiology and Camilla Merten, Institute of Immunology, Otto-von-Guericke University, Magdeburg for their expert technical assistance. The authors also acknowledge the Deutsche Forschungsgemeinschaft (DFG) for the support through the grants FOR 521-HA3498/1-2 and SPP 1128 ZU59/5-1/2.